MATERIALS SCIENCE

A bistable and reconfigurable molecular system with encodable bonds

Chunyang Zhou[1,2,3]†, Donglei Yang[1]†, Sebastian Sensale[4]†, Pranav Sharma[4], Dongfang Wang[2]‡, Lei Yu[2]§, Gaurav Arya[4], Yonggang Ke[2,5]*, Pengfei Wang[1]*

Molecular systems with ability to controllably transform between different conformations play pivotal roles in regulating biochemical functions. Here, we report the design of a bistable DNA origami four-way junction (DOJ) molecular system that adopts two distinct stable conformations with controllable reconfigurability by using conformation-controlled base stacking. Exquisite control over DOJ's conformation and transformation is realized by programming the stacking bonds (quasi–blunt-ends) within the junction to induce prescribed coaxial stacking of neighboring junction arms. A specific DOJ conformation may be achieved by encoding the stacking bonds with binary stacking sequences based on thermodynamic calculations. Dynamic transformations of DOJ between various conformations are achieved by using specific environmental and molecular stimulations to reprogram the stacking codes. This work provides a useful platform for constructing self-assembled DNA nanostructures and nanomachines and insights for future design of artificial molecular systems with increasing complexity and reconfigurability.

INTRODUCTION

In nature, molecular systems generally adopt distinct conformations to execute diverse biochemical functions (*1*, *2*). Dynamic transformation between these conformations in response to external cues enriches their functional diversity. While building artificial molecular systems that mimic, and ultimately exceed, the structural sophistication and functional diversity of natural systems holds enormous potential for applications in areas such as synthetic biology (*3*, *4*), biomedical science (*5*, *6*), and molecular computing (*7*, *8*), the realization of such task remains a long-standing challenge to this date.

The rapid development of DNA nanotechnology has led to the invention of a rich diversity of self-assembled molecular systems with increasing size, complexity, and function (*9*–*21*). Among these systems, dynamic DNA nanostructures have emerged as a class of synthetic molecular systems exhibiting unprecedented complexity and functionality (*22*–*26*), which have been extensively used for applications in material fabrication (*27*–*31*), drug delivery (*32*, *33*), and biosensing (*34*–*36*). The basis of complex DNA self-assembly lies in the simple but classical base pairing rules established in the seminal work of Watson and Crick (*37*): adenine (A) pairs with thymine (T) and cytosine (C) pairs with guanine (G). This base pairing enforces binding specificity between DNA molecules, while base stacking is essential for further stabilization of the double-helical conformation (*38*). Complementary base pairing has been the predominant strategy used for designing and modulating the self-assembly and dynamic behaviors of DNA molecular systems, while the utilization of base stacking for programming assembly has been rarely explored (*39*–*43*). The reason is clear: Unlike base pairing, which involves two types (A-T and G-C) of heterophilic attraction (like-unlike), base stacking is homophilic (like-like), and thus, it lacks specificity, rendering this mechanism much less programmable. Nonetheless, it is possible to program DNA self-assembly with base stacking based on the concept of geometry matching: The geometry of DNA nanostructures generates differential between intended and unwanted binding (*40*–*42*).

Our work is to show that additional programmability in base stacking–driven self-assembly can be achieved in dynamic and reconfigurable DNA nanostructures, through a strategy of conformation-controlled base stacking: The conformations of nanostructures are designed in ways that base stacking can only occur in limited and intended arrangement. To this end, a DNA origami molecular system inspired by DNA Holliday junctions (HJs) is designed. HJs represent one elegant natural molecular system that harvests both DNA base pairing and base stacking properties for conformation regulation. HJs contain four interconnected double-helical arms held by base pairing, which exhibit open and stacked conformations mediated by coaxial base stacking between adjacent arms (Fig. 1A) (*44*). Here, we introduce the design of a bistable and reconfigurable DNA origami four-way junction (DOJ) that structurally resembles an HJ. It contains four interconnected rectangular arms with eight stacking bonds placed at the interior edge of each arm. The pairwise coaxial stacking between neighboring arms enables the folding of two possible stable conformations. Programmable control over DOJ conformation is realized via stepwise activation of stacking bonds or via encoding stacking bonds with 4-bit

[1]Institute of Molecular Medicine, Department of Laboratory Medicine, Shanghai Key Laboratory for Nucleic Acid Chemistry and Nanomedicine, Center for DNA Information Storage, State Key Laboratory of Oncogenes and Related Genes, Renji Hospital, School of Medicine, Shanghai Jiao Tong University, Shanghai 200127, China. [2]Wallace H. Coulter Department of Biomedical Engineering, Georgia Institute of Technology and Emory University, Atlanta, GA 30322, USA. [3]College of Life Sciences and Technology, Changchun University of Science and Technology, Changchun 130013, Jilin, China. [4]Thomas Lord Department of Mechanical Engineering and Materials Science, Duke University, Durham, NC 27708, USA. [5]Department of Chemistry, Emory University, Atlanta, GA 30322, USA.
*Corresponding author. Email: pengfei.wang@sjtu.edu.cn (P.W.); yonggang.ke@emory.edu (Y.K.)
†These authors contributed equally to this work.
‡Present address: School of Biomedical Engineering and Suzhou Institute for Advanced Research, University of Science and Technology of China, Suzhou 215123, Jiangsu, China.
§Present address: The State Key Laboratory of Refractories and Metallurgy, The Institute of Advanced Materials and Nanotechnology, Wuhan University of Science and Technology, Wuhan 430081, Hubei, China.

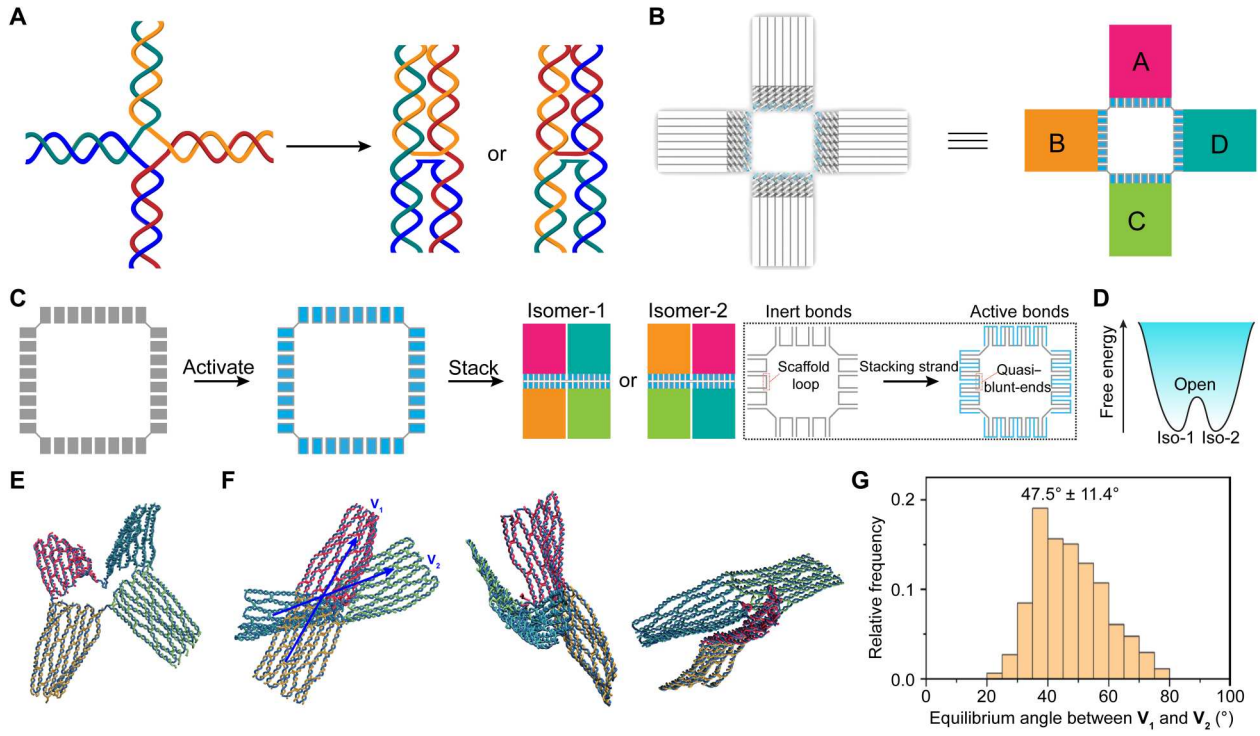

Fig. 1. Design of DOJ. (**A**) A HJ is a natural bistable molecular system whose stacked form has two stable conformations when double-helical arms coaxially stack via base stacking. (**B**) Our DNA origami four-way junction (DOJ) consists of four inter-bridged rectangular arms that structurally resembles an HJ. Each arm is one-helix tall, eight-helix wide, and 100–base pair long. (**C**) DOJ exhibits two distinct conformational isomers via quasi–blunt-end stacking, arbitrarily denoted as Isomer-1 (Iso-1; AB-CD) and Isomer-2 (Iso-2; AD-BC), respectively. The arm contains a number of eight stacking bonds. Inert stacking bonds become active when stacking strands pair with the single-stranded scaffold DNA-forming quasi–blunt-ends. (**D**) Simplified schematic of the free energy landscape of the bistable DOJ. The two global energy minima corresponding to the two stacked states are separated by an energy barrier corresponding to the open state. (**E**) Coarse-grained (oxDNA) simulations of an open DOJ. (**F**) Simulation of a stacked DOJ viewed from various angles. The simulation reveals out-of-plane angle between stacked arms. This angle can be tracked by means of vectors $\mathbf{V}_1$ and $\mathbf{V}_2$, defined by the center beads of the stacked arms. (**G**) Histogram of equilibrium angle between the stacked arms of a DOJ derived from simulations.

binary stacking sequences. Most notably, dynamic transformation between open and stacked DOJ, and between various stacked conformations, may be effectively executed by inducing specific stimulations.

RESULTS

Design, assembly, and characterization of DOJ

Our DOJ structure consists of four structurally identical single-layer rectangular arms bridged by a scaffold linkage (Fig. 1B and fig. S1), with each arm being one-helix tall, eight-helix wide, and 100–base pair long. These arms are arbitrarily denoted as A, B, C, and D, respectively. Single-stranded DNA (ssDNA) scaffold loops are placed at the interior edge of the arm, serving as inert stacking bonds. Short DNA stacking strands complementary to the scaffold DNA may be added to activate the stacking bonds by forming double-stranded quasi–blunt-ends (Fig. 1C). For a canonical DNA blunt-end, both strands come to an end at the edge. Well here in our design, the scaffold DNA has no end, as it is linked to an adjacent bond, which is thus termed as quasi–blunt-end. Because the arm is composed of eight helixes, therefore, there are a number of eight stacking bonds for each arm. The unique sequence of each DNA scaffold loop enables independent control over the activation of stacking bonds, but note that, in the current system, each stacking strand is able to activate two adjacent bonds at the same time as a staple loop of the stacking strand is intentionally designed to stabilize the stacking edge, which may be divided into two stacking strands if independent control of individual stacking bonds is necessary. Upon activation of stacking bonds, DOJ adopts two thermodynamically stable conformations when arms coaxially stack, making it a bistable molecular system (Fig. 1D). The structure is arbitrarily named as Isomer-1 (Iso-1) when A stacks to B and C stacks to D, while the stacking structure of AD and BC is named as Isomer-2 (Iso-2). Stacking between A and C or B and D is structurally prohibited because of physical constraints. Coarse-grained molecular dynamics simulations using oxDNA software (*45*) were performed to predict the molecular configurations of the open (Fig. 1E) and stacked DOJs (Fig. 1F). The simulations revealed that the pair of stacked arms are not coplanar, exhibiting an equilibrium out-of-plane angle of 47.5° (Fig. 1G).

The DOJ molecular system was subject to a one-pot thermal annealing reaction in aqueous buffer containing 12 mM Mg^{2+}. Native agarose gel electrophoresis suggested the formation of open and stacked DOJs because distinct bands of apparent retarded mobility compared to the M13 scaffold DNA were observed (Fig. 2A). Atomic force microscopy (AFM) unambiguously confirmed the assembly of DOJs in open (Fig. 2B) and stacked conformations (Fig. 2C). Because of the out-of-plane angle between stacked

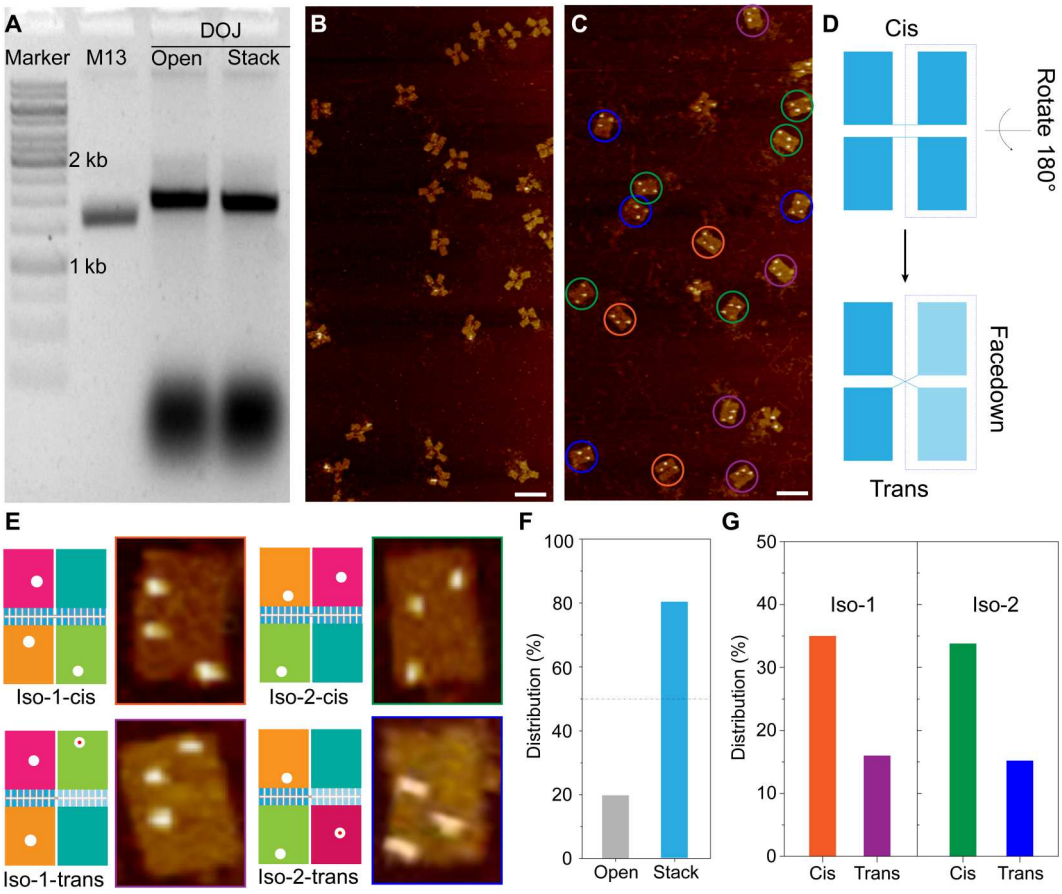

Fig. 2. Assembly and characterization of DOJ. (**A**) Native agarose gel electrophoresis of DOJs in open and stacked conformations. (**B**) Atomic force microscopy (AFM) images of open DOJs. Scale bar, 100 nm. (**C**) AFM images of stacked DOJs. Isomers are identified and highlighted by color circles. Streptavidin is anchored at designated locations on A, B, and C to discriminate between DOJ isomers. Scale bar, 100 nm. (**D**) Schematic illustration of cis and trans conformations of DOJ isomers after landing on a flat surface. Because arms are not coplanar, two possible conformations of each isomer may be observed under AFM depending on the landing angle. (**E**) Representative AFM images of various conformations. Streptavidin is illustrated as a white solid circle (faceup) or a white solid circle with red center (facedown). (**F**) Distribution of open versus stacked DOJs after stacking bonds are fully activated (N = 82). (**G**) Distribution of conformational isomers among stacked DOJs (N = 73).

arms, each isomer may adopt two possible conformations when landing onto a flat surface for AFM imaging (fig. S2), which are denoted as cis and trans, respectively (Fig. 2D). To distinguish between these conformations, streptavidin (STV) was docked onto designated locations on arms of A, B, and C through biotinylated DNA capturing strands. Modification of STV onto the rectangular origami surfaces showed no observable interference on the stacking behaviors of DOJs (fig. S3). Isomers were identified on the basis of STV arrangement patterns and highlighted by colored circles (Fig. 2C). Representative zoom-in AFM images are shown in Fig. 2E. Quantitative analysis of AFM images revealed that ~80% of the DOJs were successfully stacked when stacking bonds were fully activated (Fig. 2F). Among stacked DOJs, Iso-1 and Iso-2 were roughly equally distributed, which is consistent with the absence of asymmetries specifically introduced to favor any specific stacking pattern in the design of the structure. Further statistical analysis revealed a higher percentage (70%) of cis conformations for DOJ isomers of Iso-1 and Iso-2 after landing on a flat surface than their trans counterparts (30%) (Fig. 2G and fig. S4). This result is in good agreement with simulations, as an acute out-of-plane angle of 47.5° between stacked pairs shall lead to higher percentage of DOJ in cis conformation while landing on the surface (fig. S2). The current strategy, solely based on coaxial stacking, lacks the capability to produce DOJs in a particular cis or trans conformation. To accommodate this limitation, bridging DNA strands may be introduced on the sides of adjacent arms to either prohibit flipping (for cis conformation) or induce flipping (for trans conformation), enabling the assembly of DOJs with one specific conformation (figs. S5 to S10).

Controlling DOJ conformations via stepwise activation of stacking bonds

When stacking bonds are activated simultaneously, the DOJ unbiasedly adopts two coaxial stacking patterns and yields equally distributed isomers. In certain scenarios, such as the riboswitch-mediated regulation of protein production from an RNA transcript (*46*), precise control over the conformation of a molecular system can be of outmost importance. Here, we developed a strategy to stepwise activate stacking bonds of the DOJ so as to program its stacking pattern (Fig. 3). An open DOJ was first assembled with inert stacking bonds. Stacking strands were then added sequentially to activate the designated stacking bonds. We found that sequential activation

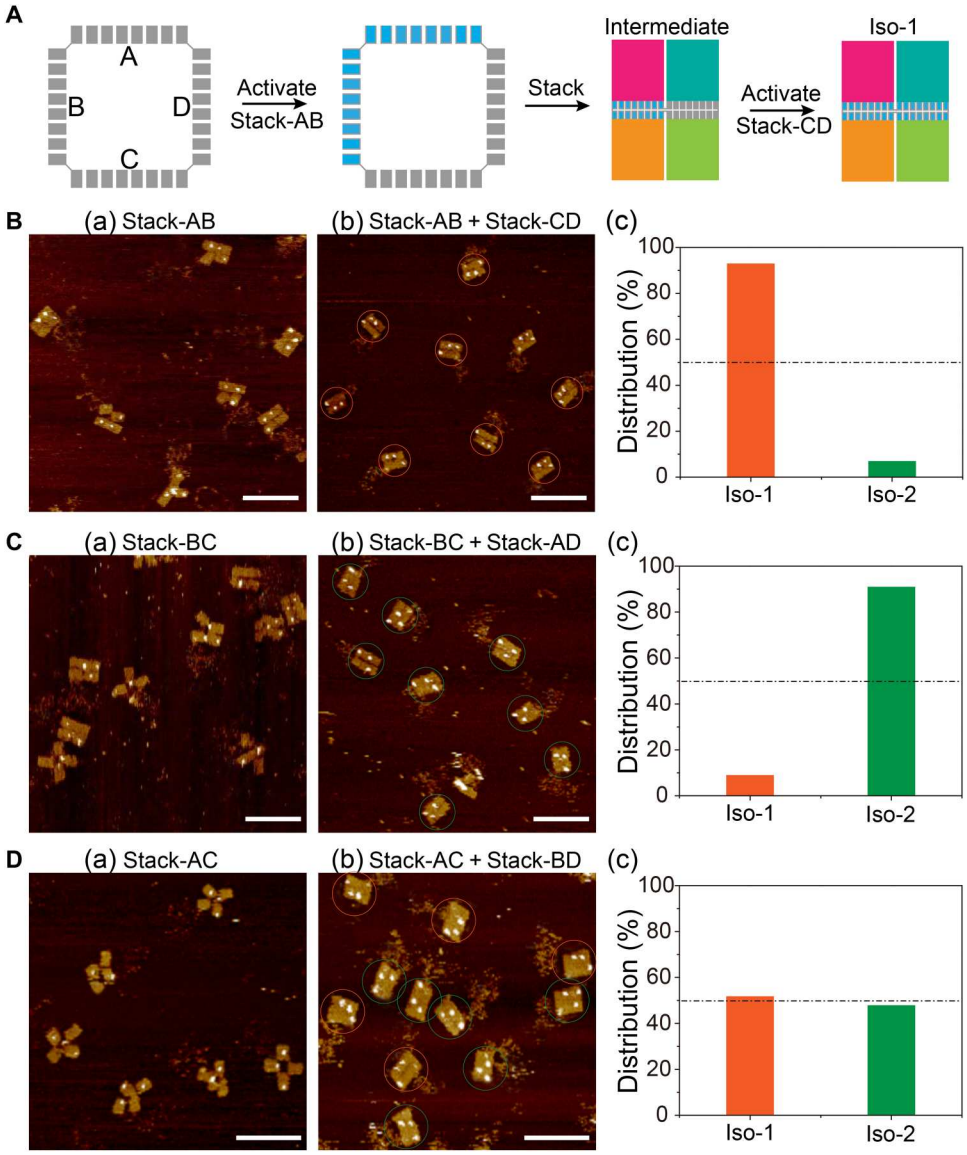

Fig. 3. Controlling DOJ conformations via stepwise activation of stacking bonds. (**A**) Stepwise activation of stacking bonds facilitates the stacking of DOJ toward a prescribed isomer, Iso-1 in this illustration. (**B**) AFM imaging of Iso-1. (a) Stack-AB is first added to activate stacking bonds on A and B forming partially stacked intermediate structure. (b) Stack-CD is subsequentially added to enable the stacking between C and D forming a fully stacked DOJ of Iso-1 conformation. (c) Quantitative analysis of DOJ isomers (N = 72). (**C**) AFM imaging of Iso-2. (a) Stack-BC is first added to activate stacking bonds on B and C forming a partially stacked intermediate structure. (b) Stack-AD is subsequentially added to enable the stacking between A and D, leading to the formation of a fully stacked DOJ of Iso-2 conformation. (c) Quantitative analysis of DOJ isomers (N = 55). (**D**) AFM imaging of DOJs with no favorable conformation. (a) Stack-AC is first added to activate stacking bonds on A and C, which cannot induce stacking because AC stacking is prohibited because of physical constrain. (b) Stack-BD is added to activate stacking bonds on B and D. With all stacking bonds activated, the DOJ may stack to form Iso-1 and Iso-2 in equal proportions, same as in the one-pot reaction scenario. (c) Quantitative analysis of DOJ isomers (N = 64). Scale bars, 100 nm.

of stacking bonds modulates the stacking pathway of the DOJ, defining its final conformation. For instance, as illustrated in Fig. 3A, stack-AB is first added to induce the stacking between A and B. The subsequent addition of stack-CD leads to the formation of Iso-1. In contrast, to produce Iso-2, a sequential order of adding stack-BC and then stack-AD may be used. AFM imaging revealed the successful formation of prescribed intermediates and stacked DOJ of desired conformations (Fig. 3, B and C, and figs. S11 and S12). Quantitative analysis of AFM images showed that ~90% of stacked DOJs were in the targeted conformation, suggesting the potency of stepwise activation strategy for conformational control. Alternative stepwise activation pathways for Iso-1 (CD-AB) and Iso-2 (AD-BC) showed comparable robustness on programming the conformation of DOJ (fig. S13). In contrast, because stacking between AC or BD is prohibited because of physical constrains in the junction design, sequential activation of AC and BD (or BD and AC) led to no preferential control over DOJ's conformation (Fig. 3D and fig. S14).

Controlling DOJ conformations by encoding stacking bonds

Previous study by Woo and Rothemund (*39*) demonstrated that binary stacking sequences composed of active and inactive stacking patches on the edge of a DNA origami structure can be readily designed to program the stacking pattern between structures. Inspired from this work, here, we sought to implement binary stacking sequences in DOJ to precisely control its stacking pattern by programing the activation of stacking bonds (Fig. 4). A 4-bit binary sequence is implemented by dividing the edge into four pairs of stacking bonds. As discussed earlier, each stacking strand is designed to activated one pair of adjacent bonds simultaneously; thus, 1 bit represents two stacking bonds, with "0" and "1" representing inert and active stacking bonds, respectively (Fig. 4A). Each junction arm has its own stacking sequence; thus, the stacking code of DOJ is described by a combination of four 4-bit stacking sequences that collectively determine the stacking pattern. As illustrated in Fig. 4A, A has a stacking sequence of 0110, which pairs with B (0110) but not with D (1001) due to sequence mismatch. From a thermodynamic perspective, stacking sequences present the lowest Gibbs free energy when all blunt-ends stack, assuming that the change in Gibbs free energy is negligible for ssDNA-ssDNA (0 and 0) and ssDNA–blunt-end (0 and 1) interactions (table S1 and fig. S15). Furthermore, oxDNA simulations revealed no apparent effect of ssDNA scaffold loops on neighboring blunt-ends, implying that inert stacking bonds exhibit insignificant influence on the interactions between active stacking bonds (figs. S16 and S17). To control DOJ conformation, our strategy is to rationally encode stacking sequences to make the desired structure more thermodynamically favored than its alternative conformation (i.e., the target conformation exhibits a significantly lower Gibbs free energy than its alternative conformation when DOJ stacks from open state) (*47*). For two conformations of Iso-1 and Iso-2, their difference in free energy is given by $\Delta\Delta G = \Delta G_1 - \Delta G_2 = (G_{Iso1} - G_{open}) - (G_{Iso2} - G_{open}) = G_{Iso1} - G_{Iso2}$. As negative values of $\Delta\Delta G$ favor the formation of Iso-1, whereas positive values favor the formation of Iso-2, we may tune our design to target conformation Iso-1 by making $\Delta G_1 = G_{Iso1} - G_{open}$ lower than $\Delta G_2 = G_{Iso2} - G_{open}$. To examine the robustness of stacking sequence for controlling DOJ conformation, we designed 12 different stacking codes (Fig. 4B), numbered in the order of decreasing value of $\Delta\Delta G$ (table S2), with all codes favoring the formation of Iso-1. One-pot assembly was carried out with corresponding stacking strands added together with scaffold DNA and structure-forming staple DNAs. AFM imaging was conducted to visualize DOJ conformations (figs. S18 to S29). Quantitative analysis revealed that the yield of stacked DOJs was positively related to the number of active stacking bonds being implemented into the codes (Fig. 4C), which was expected because a higher number of blunt-ends shall potentially induce stronger stacking forces and, thus, a higher overall yield of stacked DOJ. $\Delta\Delta G$ values of stacking codes and their corresponding yields of Iso-1 are plotted in Fig. 4 (D and E, respectively). As expected, the percentages of Iso-1 conformations were found to be above 50% for all codes, suggesting Iso-1 to be the favorable conformation. A general trend is that stacking codes of lower $\Delta\Delta G$ lead to higher percentages of Iso-1, with codes 10, 11, and 12 showing percentages as high as ~90%, suggesting the viability of tuning stacking sequences to control DOJ conformation. Note that code 5 showed unexpected poor control over DOJ conformation, whose yield of Iso-1 is much lower than that of code 2, with code 2 having the same number of active stacking bonds but a higher $\Delta\Delta G$ value. We suspect that this may be attributed to the physical locations of stacking bonds along the arm edge. Because of structural constrain, the stacking between edges shall follow a zipping mechanism, which means the stacking is initiated from the bonds placed in the corners. For code 5, the zipping process may start either way to yield Iso-1 or Iso-2. Well in contrast, the zipping process in code 2 prefers to go toward Iso-1 given that stacking bonds at other adjacent corners are missing. Furthermore, code 6 through code 9 yielded a bit lower Iso-1% than expected, suggesting that other factors besides Gibbs free energy difference and physical locations of bonds may also be involved in the stacking process. Another factor that may play a role here is the binding energy difference of stacking strands and the scaffold loops across various stacking bonds. This difference will lead to temporal variations regarding stacking bond activation, which may affect the stacking process. In general, although the stacking codes may be thermodynamically programmed to favor one specific conformation, kinetic traps toward the other conformation due to physical locations of bonds and stacking strand sequence differences cannot be fully dismissed unless specifically designed.

As stacking forces between blunt-ends are highly dependent on base pair sequences (*47*), we then wanted to program the value of $\Delta\Delta G$ through the design of base pair sequences with solely active bonds. As illustrated in Fig. 4F, three codes with different $\Delta\Delta G$ values were designed, with code 13 exhibiting no preference to either conformation, whereas code 14 and code 15 favored the conformations of Iso-1 and Iso-2, respectively. The sequence control of blunt-ends were realized by shifting the DNA scaffold by introducing scaffold loops of certain bases long within the structure main body until the desired sequence was met. AFM imaging of stacked DOJs again revealed excellent control over DOJ conformation based on differences in stacking units in the blunt-end base pair sequences (Fig. 4G and figs. S30 to S32).

Dynamic transformation of DOJ

Many molecular systems are capable of changing their conformation upon external stimulation. So far, we illustrated how a DOJ can readily transform from open to stacked conformation when stacking bonds are activated (Fig. 3). We now sought to demonstrate transformations in DOJs through changes in temperature or cation concentration, which are known to alter the stability of DNA blunt-end stacking (Fig. 5A), as previously reported by Dietz and colleagues (*41*). We showed that stacked DOJs can be opened at elevated temperature of 53°C without inducing apparent structural damage (fig. S33) and regain stacking when the temperature drops (25°C), as illustrated in Fig. 5B. This transformation process may run in multiple cycles by alternatingly increasing and decreasing the temperature (Fig. 5C). Similarly, reversible transformation may also be achieved by mediating Mg^{2+} concentration (Fig. 5, D and E), as high levels of Mg^{2+} (12 mM) favor stacking, while low levels (5 mM) favor opening.

We then attempted to induce the transformation between stacked DOJ isomers. An open-recode-stack strategy was developed, where initially stacked DOJs open up at elevated temperatures, then stacking codes get recoded by adding new stacking strands, and lastly DOJs stack into different conformations when temperature drops. The principle behind this strategy is to reprogram the Gibbs free energy difference between initial and new conformations

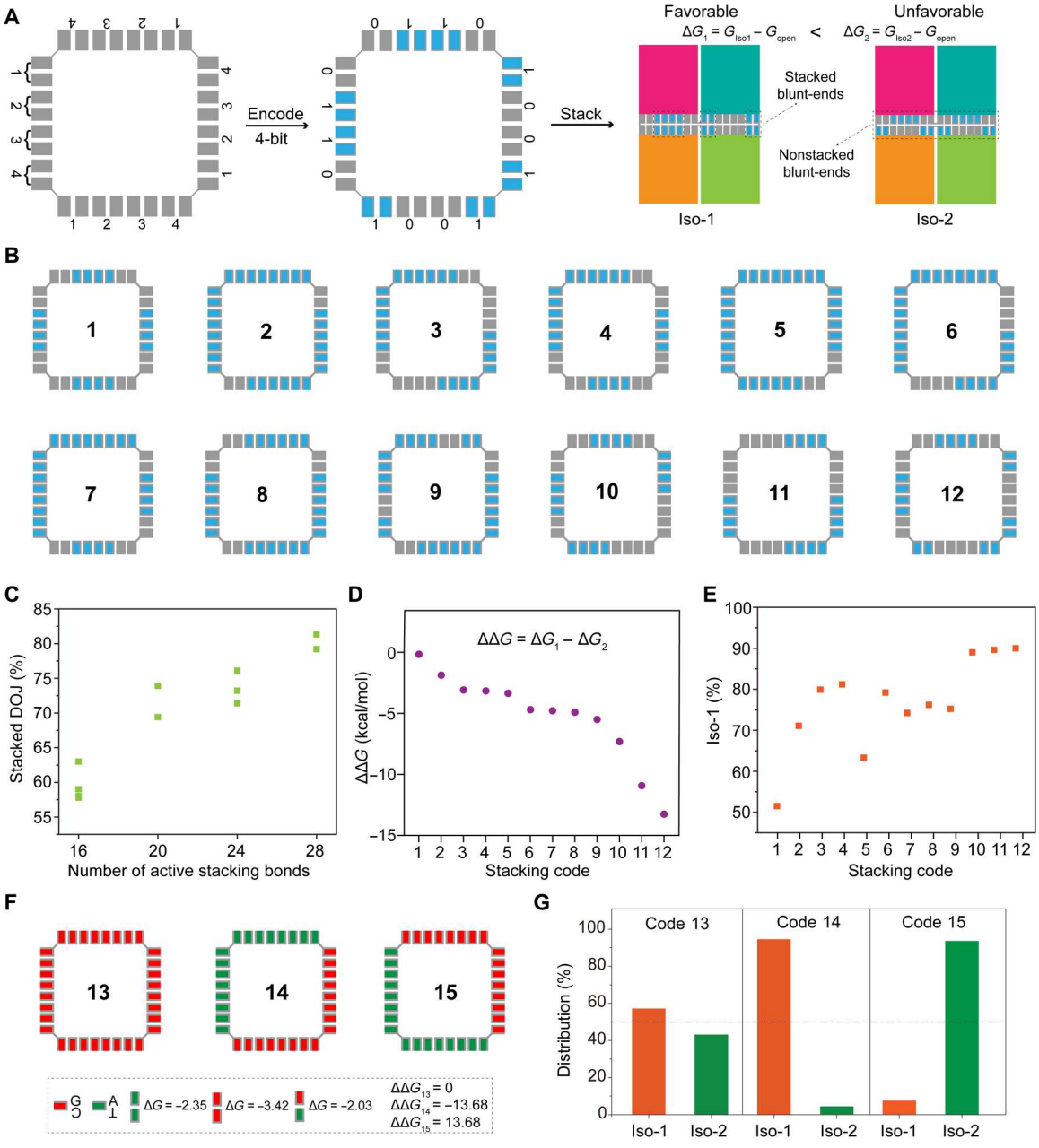

Fig. 4. Controlling DOJ conformations via encoding stacking bonds in one-pot reaction. (**A**) Scheme for programming DOJ conformations by encoding stacking bonds with 4-bit binary sequences. 0 and 1 represent inert and active stacking bonds, respectively. A stacking code contains four 4-bit binary stacking sequences that collectively determine DOJ conformation. In this illustration, Iso-1 is thermodynamically favored over Iso-2 because $\Delta G_1 < \Delta G_2$, where $\Delta G_1 = G_{Iso1} - G_{open}$, refers to the Gibbs free energy change when DOJ stacks into Iso-1 from open conformation. Similarly, $\Delta G_2 = G_{Iso2} - G_{open}$. (**B**) Twelve stacking codes of distinct stacking sequences were tested. The codes are designed and numbered in the order of increasing Gibbs free energy difference between Iso-1 and Iso-2, with all 12 codes favoring the formation of Iso-1. (**C**) Yield of stacked DOJ is positively related to the number of available active stacking bonds in the codes. (**D**) $\Delta\Delta G$ values of the 12 stacking codes. $\Delta\Delta G$ is negative for all codes, whose absolute value gradually increases in the order of code numbers. (**E**) Yield of Iso-1 for various stacking codes. In general, Iso-1% is negatively related to the value of $\Delta\Delta G$, with larger absolute value of a negative $\Delta\Delta G$ yielding higher Iso-1%. (**F**) Three stacking codes with the same stacking sequences but different blunt-end base pairs. (**G**) Quantitative analysis of conformational isomers of stacked DOJ when using codes 13, 14, and 15. (N = 135, 138, and 110, respectively).

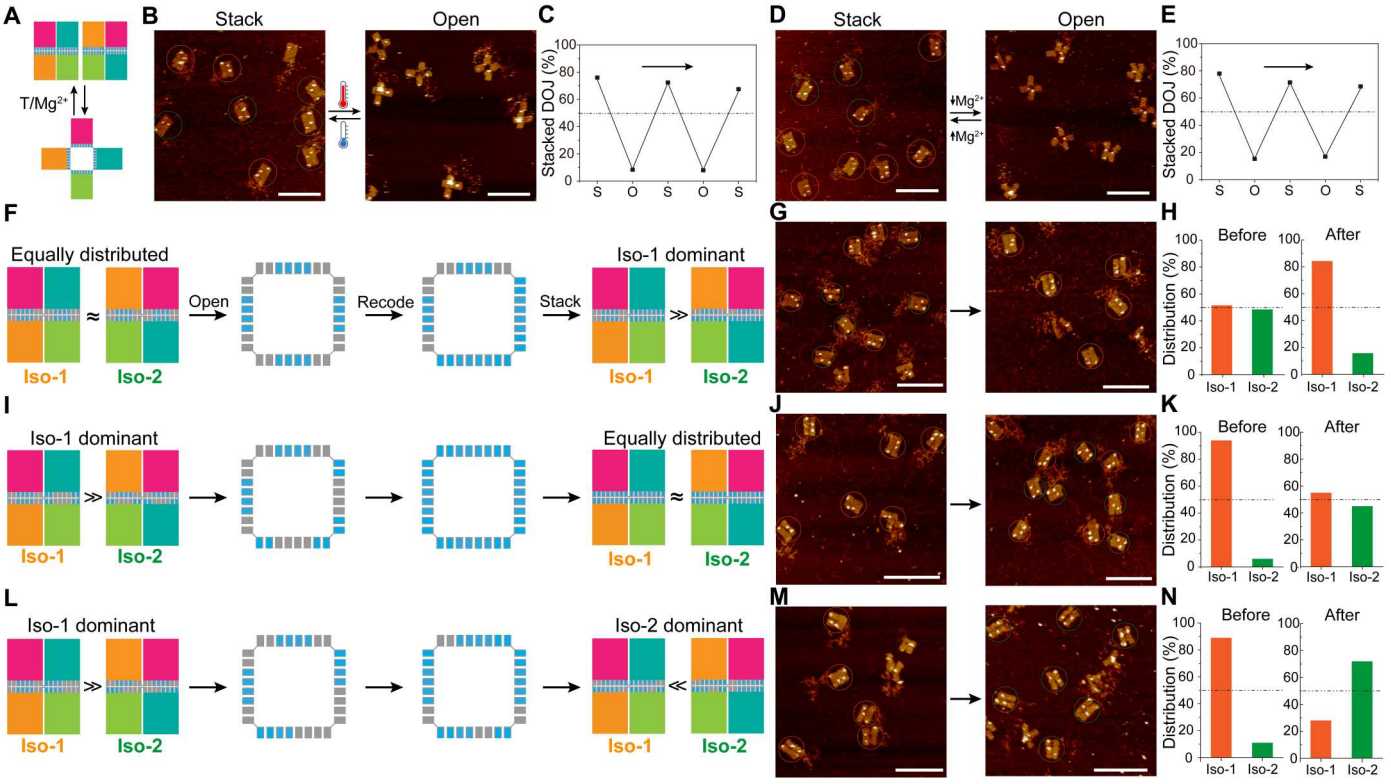

Fig. 5. Dynamic transformation of DOJ. (**A**) Reversible transformation between stacked and open DOJs by changing temperature or Mg^{2+} concentration. (**B** and **C**) Temperature-mediated reversible transformation between stacked and open DOJs. DOJs open at high temperatures (53°C), stack at low temperatures (25°C). (**D** and **E**) Mg^{2+}-mediated reversible transformation between stacked and open DOJs. DOJs opens at low level of Mg^{2+} (5 mM), stack at high level of Mg^{2+} (12 mM). (**F** to **H**) DOJs transform from mixed conformations to Iso-1–dominant conformations via an open-recode-stack strategy. Stacked DOJs are first opened at elevated temperature; stacking strands are added to recode the stacking bonds on top of initial code to shift the thermodynamic preference toward the new conformation and to open DOJ stack into the new conformations when temperature drops. (**I** to **K**) DOJs transform from Iso-1–dominant conformations to mixed conformations. (**L** to **N**) DOJ transform from Iso-1–dominant conformations to Iso-2–dominant conformation. All scale bars, 100 nm.

by recoding the stacking bonds to shift the thermodynamic preferences toward the new conformation. By implementing this protocol, we realized three types of transformations: (i) DOJs transform from mixed conformations to Iso-1–dominant conformations (Fig. 5, F to H). (ii) DOJs transform from Iso-1–dominant conformations to mixed conformations (Fig. 5, I to K). (iii) DOJs transform from Iso-1–dominant conformations to Iso-2–dominant conformation (Fig. 5, L to N). AFM imaging of DOJs confirmed the prescribed transformations (figs. S34 to S37), with the first and second types of transformations exhibiting high efficiency. The relative low conversion efficiency of the third type of transformations may be attributed to the design limitations of the current recoding method because the existing active bonds cannot be removed, hindering the design space for recoding and increasing the chances of kinetically trapping DOJs in wrongly stacked conformations. Future designs that allow erasing current codes (e.g., toehold-mediated strand displacement reactions; fig. S38) may largely boost the design space for code reprogramming to enable robust, versatile, and efficient transformations of DOJs.

DISCUSSION

One ultimate goal of molecular assembly is to construct artificial molecular systems that can resemble and eventually exceed the complexity and versatility of natural systems. DNA nanotechnology is arguably the most powerful and versatile assembly technique for building these advanced molecular systems. Here, our work was inspired by designing a bistable and reconfigurable DOJ molecular system that mimics the HJ from a structural perspective. Molecular recognition was implemented by placing blunt-end based stacking bonds to induce intramolecular stacking and stabilize specific conformational states of the structure. Exquisite control over conformation was realized by stepwise activation of stacking bonds or by encoding stacking bonds with 4-bit binary stacking sequences. The encoding mechanisms are grounded on thermodynamic free energy calculations to code the stacking bonds in temporal activation order, in spatial arrangements, or in blunt-end base pair sequences. A targeting conformation can be favorably produced if it has lower Gibbs free energy than its competing alternative conformation. Most notably, DOJs exhibited dynamic reconfigurability that can transform between various conformations following programmable pathways. There are several advantages accompanying the current design strategy. First, unlike previously reported geometry-matched base stacking methods, DOJs use conformation-controlled base stacking that renders it exhibiting improved programmability. Second, DOJs contain multiple arms that can pairwise interact to produce various distinct conformations from a single module. Third, stacking bonds are implemented and

embedded within the junction, prohibiting nonspecific intermolecular stacking between junction modules. Last, because pairwise intracellular interactions within the junction module exhibit minimal external interference, it may readily serve as a platform to directly study competing interactions in a highly unbiased and comparable manner. We envision that the design space of DOJs may be drastically expanded either by increasing the number of stacking bonds or the number of arms or by building higher-order assemblies out of basic DOJ units (fig. S39). With such a high potential in design space, we aspire that a variety of molecular systems with sophisticated structure, dynamic capability, and versatile functions may be developed in the future.

MATERIALS AND METHODS

Materials

Single-stranded M13 bacteriophage DNAs (p7560) were produced following a previously published protocol (*48*). The DNA staple strands (table S3) were purchased from Integrated DNA Technologies or from Sangon Biotech.

Computational simulation of DOJ

Distribution of angles between stacking components

The DOJ device was built in caDNAno (*49*) as shown in fig. S1. This structure was converted to oxDNA (*45*) using the tacoxDNA Python package (*50*), minimized on the oxDNA.org server (*51*), and simulated by running coarse-grained molecular dynamics simulations with the oxDNA force field on graphics processing units (GPUs). A john thermostat was used, which emulates Brownian dynamics. The number of steps between velocity refresh attempts (Newtonian steps) was set to 103, and the overall monomer diffusion coefficient resulting from the thermostat was 2.5. Simulations were performed at 37°C and at a high salt concentration typical of origami studies, $[Na^+] = 0.5M$ (*52*). Interactions were modeled with the DNA2 force field (*53*) using the average sequence model, and a time step of 0.001 oxDNA time units (3.03 fs) was used. The structures were equilibrated for 1,000,000,000 steps, and a production stage consisting of 2,000,000,000 steps (approximately 30.30 μs) followed this equilibration. Coordinates of all atoms were outputted every 97,680 steps.

Effects of inactive patches in binding dynamics

To assess whether inactive patches (inert stacking bonds) influence the thermodynamics of binding of our stacking components, coarse-grained simulations of these patches were performed using oxDNA on tile structures specifically designed for the study of blunt-end stacking interaction (*39*). As this structure is quite curved in nature, we analyzed four different locations of these active patches to evaluate the dependence of patch dynamics on local shape. While oxDNA allows the user to access longer time scale (*54*), capturing binding events is still inaccessible to this model, and thus, we restrict ourselves to analyzing the effect of inactive patches in equilibrium properties of the active ones, by comparing simulations of two tiles, one with inactive patches in between the active patches and one without.

After conversion of the origami designs to the oxDNA model by means of tacoxDNA, the structures were first relaxed with a 10,000-step Monte Carlo simulation at 20°C, with the maximum force allowed on the DNA backbone set to 243.15 pN. This was followed by a 1,000,000-step molecular dynamics relaxation, with the same backbone force constraint. A Langevin thermostat was used to maintain the system at 20°C, and a time step of 0.002 oxDNA time units (roughly 6.06 fs) was used. Both for equilibration and measurement MD runs, the backbone force constraint was removed, and the time step was increased to 0.005 oxDNA units (~15.15 fs); the equilibration was performed over 280,000,000 steps, and measurement was over 424,000,000 steps. As in the previsous section, a high monovalent salt concentration of 0.5 M was used, and the overall monomer diffusion coefficient was 2.5. The number of steps between velocity refresh attempts (Newtonian steps) was set to 103, and interactions were modeled with the DNA2 force field using the average sequence model (*53*). For equilibrium analysis of active and inactive patches, coordinates of the tile structures were output every 10,000,000 steps.

Using a homemade code, vectors u1, u2, u3, v1, v2, and v3 were computed for each of the four sets of patches in our systems [see fig. S16B (inset)] for each frame outputted (note that vector v2 is not defined for the tile without inactive patches). The angle between v1 and v3 approximates the angle in between the active patches. The out-of-plane angles between these vectors and the tiles may be estimated from their dot product with the vector normal to the plane established by u1 and u3, as these vectors locally define the body of the tile. The angles between u1 and v1 and between u3 and v3 were also tracked, as these angles provide information of the in-plane deviation of the blunt-ends. Figure S16 compares these three metrics across the structure with inactive patches (dashed) and the one without them (solid), showing that the scaffold loop does not affect the equilibrium behavior of the active patches, as expected.

Further examining the system with inactive patches, the minimum bounding sphere of the bases in the inactive patch was tracked, as well as the shortest distance between any base in the inactive patch and any base in either of the neighboring active patches (fig. S17). Last, the angle that each of the three patches takes with respect to the body of the tile is plotted as a function of time. From these results, it becomes clear that the inactive patch remains physically distant from the active patches (most often ~3 nm) and remains at an ~20° angle offset from the active patches.

Preparation of DOJ

DOJ was designed using caDNAno. In a typical sample preparation, staples were mixed with ssDNA scaffold (p7560, 10 nM) in fivefold molar excess in folding buffer [5 mM tris, 1 mM EDTA, and 12 mM magnesium chloride (pH 8.0)] with total volume of 50 μl. The mixed solution was annealed in a thermocycler programmed for a cooling ramp from 85° to 25°C in the following protocol: 85°C for 5 min, 65° to 25°C, at 1 min/0.1°C. After the formation of open DOJ, designated DNA stacking strands were added in threefold molar excess of folding staples and incubate at room temperature for 5 hours. In the meantime, streptavidin was added to the mixture in a 10-fold molar excess of staples. DNA locking strands (L_{AB}, L_{BC}, L_{AC}, and L_{BD}) were introduced onto designated arms to avoid or to induce flipping of stacked arms to control DOJ at one particular conformation.

Agarose gel electrophoresis

DOJ was subject to 1% native agarose electrophoresis for about 2 hours at 70 V in ice bath [the prepared gel in 0.5× tris-borate EDTA buffer was supplemented with 12 mM $MgCl_2$ and 0.005%

(v/v) ethidium bromide]. Twenty microliters of 10 nM DOJ was loaded into the gel. Next, the target gel bands were excised and placed into a Freeze 'N Squeeze column (Bio-Rad Laboratories Inc.). The gel pieces were crushed into fine pieces by a microtube pestle in the column and then centrifuged at 7000*g* for 5 min. Samples that were extracted through the column were collected for AFM imaging.

AFM imaging

AFM images were obtained using an SPM MultiMode with Digital Instruments NanoScope V controller. Three microliters of purified samples (~3 nM DOJ) were deposited onto freshly cleaved mica (diameter, 9.5 mm; SPI Supplies) for imaging. After sample adsorption for approximately 2 min, 80 μl of 0.5× Tris-EDTA (10 mM $MgCl_2$) and 2 μl of $NiCl_2$ (100 mM) were then added onto the mica. The sample was imaged in ScanAsyst mode in fluid cell. The AFM tips used were on the short and thin cantilevers in the SNL-10 silicon nitride cantilever chip.

Yield calculations

The equations to calculate the yield and ratio of each conformation were listed as follows

$$\text{Stack yield} = \frac{\mathrm{N(S)}}{\mathrm{N(O)} + \mathrm{N(S)}} \quad (1)$$

$$Yield\ (Iso-1) = \frac{N(Iso-1)}{N(S)} \quad (2)$$

In equation 1, the $N(S)$ stands for the total number of stacked DOJ used in this case. $N(O)$ stands for the number of open-state DOJ. In equation 2, yield of Iso-1 (or the yield of Iso-2) was used to represent the proportion of each correct conformation formed in all stacked DOJ. The N(Iso-1) showed the total number of stack conformation Iso-1 used in this case.

Stepwise activation of stacking bonds

In the case of the formation of Iso-1 conformations, stack-AB was first added in threefold molar excess of folding staples to open DOJ. At the same time, the streptavidin was added to the mixture in a 10-fold molar excess of folding staples and incubated at room temperature for 5 hours. In the second step, stack-CD was added with the same concentrations as stack-AB and then incubated at room temperature for another 3 hours. The same protocol was followed by all other stepwise activation combinations.

One-pot programming of the stacking bonds

By constructing an encoding system, the "one-pot" method is guided to further regulate the stacking effect of DOJ. Different from two-step activation of stacking blunt-ends, all the encoded stacking sequences were added in one-pot into the open DOJ before purification. After 3 to 5 hours incubation at room temperature, the samples were purified and ready for AFM imaging.

Dynamic transformation of DOJ

Reversible transformation from the open to stacked state by controlling the reaction temperature or Mg^{2+} concentration

First, for temperature-mediated transformation, during the reversible transformation, purified stacked DOJ was incubated at 53°C for 5 hours and then directly dropped onto the clean mica for the first open-state AFM testing. The rest sample was continuously incubated in room temperature for 3 to 5 hours. After the sample was fully stacked, it was dropped onto the mica and ready for second AFM testing. By repeating the above steps, a multistep reversible reaction can be achieved.

Second, for Mg^{2+}-mediated transformation, during the reversible transformation, the concentration of magnesium ions was reduced from 12 to ~5 mM in stacked DOJ and reacted at room temperature for 1 hours. Then, the sample was directly dropped onto the clean mica for the first open-state AFM testing. Next, the concentration of magnesium ions was increased to 12 mM and reacted at room temperature for 1 to 3 hours. After the sample was fully stacked, it was dropped onto the mica and ready for second AFM testing. By repeating the above steps, a multistep reversible reaction can be achieved.

Transform DOJ from equally distributed conformation to Iso-1–dominant conformation

The equally distributed conformations with designated stacking codes were first prepared. Next, other encoded sequences for transformation were added into it and incubated in the following protocol: 25°C for 3 hours, increase the temperature from 25 to 53°C for 3 hours, and then decrease the temperature from 53 to 25°C for 3 hours. After the sample was fully stacked, it was dropped onto the mica and ready for second AFM testing.

Transform DOJ from Iso-1–dominant conformation to equally distributed conformation or to Iso-2–dominant conformation

The Iso-1–dominant conformations with certain encoding stacking sites were prepared first of all. Next, other encoded sequences for transformation were added into it and incubated in the following protocol: 25°C for 3 hours, increase the temperature from 25° to 53°C for 3 hours, and then decrease the temperature from 53° to 25°C for 3 hours. After the sample was fully stacked, it was dropped onto the mica and ready for second AFM testing.

Thermodynamic calculation

According to the previous work on the free energy change for stacking between different blunt-ends (table S1) (*47*), we calculated and summarized the total free energy change for each stacking code, assuming that the change in Gibbs free energy, ΔG, is zero for potential loop–blunt-end and loop-loop interactions (*39*).

Supplementary Materials

This PDF file includes:

Figs. S1 to S39

Tables S1 to S3

REFERENCES AND NOTES

1. K. Henzler-Wildman, D. Kern, Dynamic personalities of proteins. *Nature* **450**, 964–972 (2007).
2. N. R. Latorraca, A. J. Venkatakrishnan, R. O. Dror, GPCR dynamics: Structures in motion. *Chem. Rev.* **117**, 139–155 (2017).
3. S. J. Culler, K. G. Hoff, C. D. Smolke, Reprogramming cellular behavior with RNA controllers responsive to endogenous proteins. *Science* **330**, 1251–1255 (2010).
4. A. A. Green, P. A. Silver, J. J. Collins, P. Yin, Toehold switches: De-novo-designed regulators of gene expression. *Cell* **159**, 925–939 (2014).
5. F. Hong, D. Ma, K. Wu, L. A. Mina, R. C. Luiten, Y. Liu, H. Yan, A. A. Green, Precise and programmable detection of mutations using ultraspecific riboregulators. *Cell* **180**, 1018–1032.e16 (2020).

6. S. M. Douglas, I. Bachelet, G. M. Church, A logic-gated nanorobot for targeted transport of molecular payloads. *Science* **335**, 831–834 (2012).
7. A. A. Green, J. Kim, D. Ma, P. A. Silver, J. J. Collins, P. Yin, Complex cellular logic computation using ribocomputing devices. *Nature* **548**, 117–121 (2017).
8. D. Woods, D. Doty, C. Myhrvold, J. Hui, F. Zhou, P. Yin, E. Winfree, Diverse and robust molecular algorithms using reprogrammable DNA self-assembly. *Nature* **567**, 366–372 (2019).
9. N. C. Seeman, Nucleic acid junctions and lattices. *J. Theor. Biol.* **99**, 237–247 (1982).
10. E. Winfree, F. Liu, L. A. Wenzler, N. C. Seeman, Design and self-assembly of two-dimensional DNA crystals. *Nature* **394**, 539–544 (1998).
11. H. Yan, S. H. Park, G. Finkelstein, J. H. Reif, T. H. LaBean, DNA-templated self-assembly of protein arrays and highly conductive nanowires. *Science* **301**, 1882–1884 (2003).
12. Y. He, Y. Tian, Y. Chen, Z. Deng, A. E. Ribbe, C. Mao, Sequence symmetry as a tool for designing DNA nanostructures. *Angew. Chem. Int. Ed. Engl.* **44**, 6694–6696 (2005).
13. P. W. K. Rothemund, Folding DNA to create nanoscale shapes and patterns. *Nature* **440**, 297–302 (2006).
14. Y. He, T. Ye, M. Su, C. Zhang, A. E. Ribbe, W. Jiang, C. Mao, Hierarchical self-assembly of DNA into symmetric supramolecular polyhedra. *Nature* **452**, 198–201 (2008).
15. S. M. Douglas, H. Dietz, T. Liedl, B. Hogberg, F. Graf, W. M. Shih, Self-assembly of DNA into nanoscale three-dimensional shapes. *Nature* **459**, 414–418 (2009).
16. J. Zheng, J. J. Birktoft, Y. Chen, T. Wang, R. Sha, P. E. Constantinou, S. L. Ginell, C. Mao, N. C. Seeman, From molecular to macroscopic via the rational design of a self-assembled 3D DNA crystal. *Nature* **461**, 74–77 (2009).
17. Y. G. Ke, L. L. Ong, W. M. Shih, P. Yin, Three-dimensional structures self-assembled from DNA bricks. *Science* **338**, 1177–1183 (2012).
18. F. Zhang, S. Jiang, S. Wu, Y. Li, Y. Liu, C. Mao, Complex wireframe DNA origami nanostructures with multi-arm junction vertices. *Nat. Nanotechnol.* **10**, 779–784 (2015).
19. P. Wang, S. Wu, C. Tian, G. Yu, W. Jiang, G. Wang, C. Mao, Retrosynthetic analysis-guided breaking tile symmetry for the assembly of complex DNA nanostructures. *J. Am. Chem. Soc.* **138**, 13579–13585 (2016).
20. G. Tikhomirov, P. Petersen, L. L. Qian, Fractal assembly of micrometre-scale DNA origami arrays with arbitrary patterns. *Nature* **552**, 67–71 (2017).
21. G. Yao, F. Zhang, F. Wang, T. Peng, H. Liu, E. Poppleton, P. Sulc, S. Jiang, L. Liu, C. Gong, X. Jing, X. Liu, L. Wang, Y. Liu, C. Fan, H. Yan, Meta-DNA structures. *Nat. Chem.* **12**, 1067–1075 (2020).
22. C. Mao, W. Sun, Z. Shen, N. C. Seeman, A nanomechanical device based on the B-Z transition of DNA. *Nature* **397**, 144–146 (1999).
23. B. Yurke, A. J. Turberfield, A. P. Mills Jr., F. C. Simmel, J. L. Neumann, A DNA-fuelled molecular machine made of DNA. *Nature* **406**, 605–608 (2000).
24. J. Song, Z. Li, P. Wang, T. Meyer, C. Mao, Y. Ke, Reconfiguration of DNA molecular arrays driven by information relay. *Science* **357**, (2017).
25. M. DeLuca, Z. Shi, C. E. Castro, G. Arya, Dynamic DNA nanotechnology: Toward functional nanoscale devices. *Nanoscale Horiz.* **5**, 182–201 (2020).
26. Y. Zhang, V. Pan, X. Li, X. Yang, H. Li, P. Wang, Y. Ke, Dynamic DNA structures. *Small* **15**, 1900228 (2019).
27. A. Kuzyk, R. Schreiber, H. Zhang, A. O. Govorov, T. Liedl, N. Liu, Reconfigurable 3D plasmonic metamolecules. *Nat. Mater.* **13**, 862–866 (2014).
28. Z. Zhang, Y. Yang, F. Pincet, M. C. Llaguno, C. Lin, Placing and shaping liposomes with reconfigurable DNA nanocages. *Nat. Chem.* **9**, 653–659 (2017).
29. C. Zhou, L. Xin, X. Duan, M. J. Urban, N. Liu, Dynamic plasmonic system that responds to thermal and aptamer-target regulations. *Nano Lett.* **18**, 7395–7399 (2018).
30. P. Zhan, M. J. Urban, S. Both, X. Duan, A. Kuzyk, T. Weiss, N. Liu, DNA-assembled nanoarchitectures with multiple components in regulated and coordinated motion. *Sci. Adv.* **5**, eaax6023 (2019).
31. A. Cangialosi, C. Yoon, J. Liu, Q. Huang, J. K. Guo, T. D. Nguyen, D. H. Gracias, R. Schulman, DNA sequence-directed shape change of photopatterned hydrogels via high-degree swelling. *Science* **357**, 1126–1130 (2017).
32. S. Li, Q. Jiang, S. Liu, Y. Zhang, Y. Tian, C. Song, J. Wang, Y. Zou, G. J. Anderson, J. Y. Han, Y. Chang, Y. Liu, C. Zhang, L. Chen, G. Zhou, G. Nie, H. Yan, B. Ding, Y. Zhao, A DNA nanorobot functions as a cancer therapeutic in response to a molecular trigger in vivo. *Nat. Biotechnol.* **36**, 258–264 (2018).
33. S. Liu, Q. Jiang, X. Zhao, R. Zhao, Y. Wang, Y. Wang, J. Liu, Y. Shang, S. Zhao, T. Wu, Y. Zhang, G. Nie, B. Ding, A DNA nanodevice-based vaccine for cancer immunotherapy. *Nat. Mater.* **20**, 421–430 (2021).
34. S. Modi, G. S. M., D. Goswami, G. D. Gupta, S. Mayor, Y. Krishnan, A DNA nanomachine that maps spatial and temporal pH changes inside living cells. *Nat. Nanotechnol.* **4**, 325–330 (2009).
35. K. Leung, K. Chakraborty, A. Saminathan, Y. Krishnan, A DNA nanomachine chemically resolves lysosomes in live cells. *Nat. Nanotechnol.* **14**, 176–183 (2019).
36. T. Funck, F. Nicoli, A. Kuzyk, T. Liedl, Sensing picomolar concentrations of RNA using switchable plasmonic chirality. *Angew. Chem. Int. Ed. Engl.* **57**, 13495–13498 (2018).
37. J. D. Watson, F. H. C. Crick, Molecular structure of nucleic acids: A structure for deoxyribose nucleic acid. *Nature* **171**, 737–738 (1953).
38. P. Yakovchuk, E. Protozanova, M. D. Frank-Kamenetskii, Base-stacking and base-pairing contributions into thermal stability of the DNA double helix. *Nucleic Acids Res.* **34**, 564–574 (2006).
39. S. Woo, P. W. Rothemund, Programmable molecular recognition based on the geometry of DNA nanostructures. *Nat. Chem.* **3**, 620–627 (2011).
40. A. Rajendran, M. Endo, Y. Katsuda, K. Hidaka, H. Sugiyama, Programmed two-dimensional self-assembly of multiple DNA origami jigsaw pieces. *ACS Nano* **5**, 665–671 (2011).
41. T. Gerling, K. F. Wagenbauer, A. M. Neuner, H. Dietz, Dynamic DNA devices and assemblies formed by shape-complementary, non–base pairing 3D components. *Science* **347**, 1446–1452 (2015).
42. K. F. Wagenbauer, C. Sigl, H. Dietz, Gigadalton-scale shape-programmable DNA assemblies. *Nature* **552**, 78–83 (2017).
43. P. Petersen, G. Tikhomirov, L. Qian, Information-based autonomous reconfiguration in systems of interacting DNA nanostructures. *Nat. Commun.* **9**, 5362 (2018).
44. D. R. Duckett, A. I. Murchie, S. Diekmann, E. von Kitzing, B. Kemper, D. M. Lilley, The structure of the Holliday junction, and its resolution. *Cell* **55**, 79–89 (1988).
45. P. Šulc, F. Romano, T. E. Ouldridge, L. Rovigatti, J. P. K. Doye, A. A. Louis, Sequence-dependent thermodynamics of a coarse-grained DNA model. *J. Chem. Phys.* **137**, 135101 (2012).
46. E. Nudler, A. S. Mironov, The riboswitch control of bacterial metabolism. *Trends Biochem. Sci.* **29**, 11–17 (2004).
47. F. Kilchherr, C. Wachauf, B. Pelz, M. Rief, M. Zacharias, H. Dietz, Single-molecule dissection of stacking forces in DNA. *Science* **353**, aaf5508 (2016).
48. S. M. Douglas, J. J. Chou, W. M. Shih, DNA-nanotube-induced alignment of membrane proteins for NMR structure determination. *Proc. Natl. Acad. Sci. U.S.A.* **104**, 6644–6648 (2007).
49. S. M. Douglas, A. H. Marblestone, S. Teerapittayanon, A. Vazquez, G. M. Church, W. M. Shih, Rapid prototyping of 3D DNA-origami shapes with caDNAno. *Nucleic Acids Res.* **37**, 5001–5006 (2009).
50. A. Suma, E. Poppleton, M. Matthies, P. Šulc, F. Romano, A. A. Louis, J. P. K. Doye, C. Micheletti, L. Rovigatti, TacoxDNA: A user-friendly web server for simulations of complex DNA structures, from single strands to origami. *J. Comput. Chem.* **40**, 2586–2595 (2019).
51. E. Poppleton, R. Romero, A. Mallya, L. Rovigatti, P. Šulc, OxDNA.org: A public webserver for coarse-grained simulations of DNA and RNA nanostructures. *Nucleic Acids Res.* **49**, W491–W498 (2021).
52. M. C. Engel, D. M. Smith, M. A. Jobst, M. Sajfutdinow, T. Liedl, F. Romano, L. Rovigatti, A. A. Louis, J. P. K. Doye, Force-induced unravelling of DNA origami. *ACS Nano* **12**, 6734–6747 (2018).
53. B. E. Snodin, F. Randisi, M. Mosayebi, P. Šulc, J. S. Schreck, F. Romano, T. E. Ouldridge, R. Tsukanov, E. Nir, A. A. Louis, J. P. Doye, Introducing improved structural properties and salt dependence into a coarse-grained model of DNA. *J. Chem. Phys.* **142**, 234901 (2015).
54. A. Sengar, T. E. Ouldridge, O. Henrich, L. Rovigatti, P. Šulc, A primer on the oxDNA model of DNA: When to use it, how to simulate it and how to interpret the results. *Front. Mol. Biosci.* **8**, 693710 (2021).

Acknowledgments: We thank M. DeLuca of Duke University for providing the MATLAB code used for rendering simulation images. **Funding**: P.W. thanks the support from National Key Research and Development Program of China (2021YFA0910100 and 2018YFA0902601) and from the National Natural Science Foundation of China (52061135109 and 21974086). Y.K. and G.A. thank the support from the Department of Energy (grant no. DE-SC0020996). **Author contributions:** C.Z. and D. Y. carried out experiments, analyzed the data, and prepared the manuscript. S.S. and P.S. conducted computational simulations. D.W. and L.Y. carried out some of the AFM imaging experiments and analyzed the data. G.A. supervised the computational aspects of the study. Y.K. and P.W. initiated the project, designed and supervised the study, interpreted the data, and prepared the manuscript. All authors revised, reviewed, and approved the manuscript. **Competing interests:** The authors declare that they have no competing interests. **Data and materials availability:** All data needed to evaluate the conclusions in the paper are present in the paper and/or the Supplementary Materials.

Submitted 7 August 2022
Accepted 20 October 2022
Published 16 November 2022
10.1126/sciadv.ade3003